Astron. Astrophys. 112, 377–385 (1982)

ASTRONOMY AND ASTROPHYSICS

The Importance of Plasma Effects on Electron-cyclotron Maser-emission from Flaring Loops

R. R. Sharma, Loukas Vlahos, and K. Papadopoulos

Astronomy Program, University of Maryland, College Park, MD 20742, USA

Received April 13, accepted May 19, 1981

SUMMARY. Electron cyclotron maser instability has been suggested as the cause of the observed short (10-20 msec), intense (~ brightness temperature ≈ 10^{15} K) and up to 100% polarized microwave solar emission. It is shown that plasma effects and thermal cyclotron damping, ignored in previous theories, play an important role in controlling the frequency range of the emission. The radio emission is suppressed for ω_e/Ω_e ratios (ω_e and Ω_e are the plasma and the cyclotron frequencies) smaller than 0.4. An examination of the cyclotron damping, reveals that the maser action is suppressed unless a large fraction (i.e. over 10%) of the accelerated electrons participates in the emission process.

Key words: Solar Radio Bursts - Cyclotron Maser - Plasma Radiation - Solar Flares.

I. INTRODUCTION

Cyclotron-maser from unstable velocity distributions has been suggested as a possible emission mechanism for radio bursts (Twiss and Roberts, 1958; Fung and Yip, 1966; Ramaty, 1969; Mangeney and Veltri, 1976; Stepanov, 1978). The interest in cyclotron-maser emission has been renewed (Holman et al., 1980; Melrose and Dulk, 1981) by a number of high time resolution observations at cm wavelength (Slottje, 1978, 1980; Kaufman et al., 1980), revealing the existence of high brightness temperature ($< 10^{15}$ K), strongly polarized (≃ 100%) spikes with time duration ≈ 10 msec. On the contrary, microwave observations with time resolution $\gtrsim$ 10 secs have a smooth time profile, duration 2-5 min, are partially polarized (10-30%) and their brightness temperature is less than 10^9 K (see Kundu and Vlahos, 1982). It appears from Figure 1 that the "spikes" observed with high time resolution are superimposed on the "smooth" component observed by the low time resolution telescopes. The "smooth" component of the burst has been interpreted (Ramaty, 1969; Takakura, 1972) as the result of gyrosynchrotron emission from the mildly relativistic electrons released in the flare and trapped in a magnetic loop with $\omega_e/\Omega_e \ll 1$. Holman et al. (1980) and Melrose and Dulk (1981) suggested that the trapped electrons could form a loss-cone velocity distribution at the foot of the magnetic loop and drive a cyclotron-maser instability resulting in the observed high brightness temperature spikes. While this scenario seems very attractive, it suffers from a difficult problem which has motivated this study.

The problem can be understood by noting that the observed power depends on two factors; the strength of the generating instability and the absorption which occurs in its propagation path towards the observer. The growth rate calculations reported by Melrose and Dulk (1981) have ignored the ambient plasma effects, by taking the ratio $(\omega_e/\Omega_e) \to 0$. In this case the ratio of the growth rate of the maser instability for the first harmonic $\omega \approx \Omega_e$, (γ_1), to that of the second harmonic $\omega \approx 2\Omega_e$, (γ_2), is of the order of ≈ 100. One would therefore expect no emission in the second harmonic, since the energy will be depleted quickly by first harmonic emission. (Note, that even for one

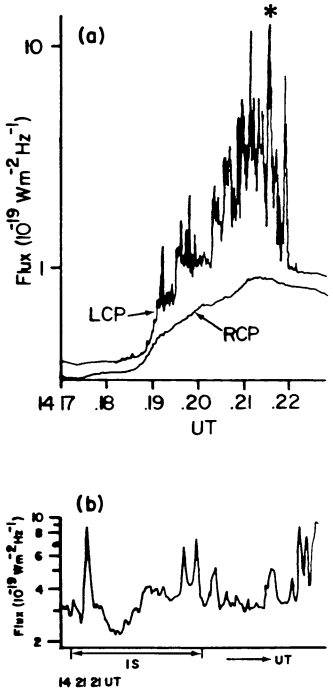

Fig. 1. (a) Flux density of left (LCP) and right (RCP) circularly polarized components of the solar burst of 1978 April 11 observed by Slottje (1978). (b) An expansion of the portion shown by an asterisk in (a) show clearly that the spikes are irregular in time with no obvious pulsation frequency.

Send offprint requests to: R. R. Sharma

growth time of $2\Omega_e$, the ratio of the intensities will be $(I_{\Omega_e}/I_{2\Omega_e}) \approx e^{100}$. However, since the radiation propagates towards weaker magnetic fields the first harmonic will be strongly absorbed in the $2\Omega_e$ layer and will not reach the observer. A possible resolution of the above dillema would require conditions relevant to the loops that could suppress the first harmonic emission, so that $(\gamma_1/\gamma_2) \lesssim 1$. In this case emission occurs at $2\Omega_e$ without being affected by the Ω_e growth. As will be shown in section 3, waves with frequency $\omega \geq 2\Omega_e$ are very weakly absorbed at the $3\Omega_e$ layer and can therefore reach the observer. It will be shown below that the previously neglected plasma effects (i.e. (ω_e/Ω_e) small but finite), actually reverse the ratio (γ_1/γ_2) from $(\gamma_1/\gamma_2) \gg 1$ for $(\Omega_e/\omega_e) > 10$ to $(\gamma_1/\gamma_2) \lesssim 1$ if $(\Omega_e/\omega_e) < 3.0$.

In the next section we discuss the flare model used in our calculation and the importance of plasma effects in the relative growth of the first and second harmonic. Section III discusses the gyrothermal absorption from a flaring loop. We emphasise the role of the magnetic field topology on the absorption or amplification of the waves emitted close to the harmonics and propagate out of the loop. Section IV examines the conditions under which high brightness sources in the Solar Atmosphere can be interpreted as the result of cyclotron-maser instabilities. The final section summarizes our results and assesses their importance in explaining the high time resolution microwave bursts.

II. IMPORTANCE OF PLASMA EFFECTS

a. The Model

We consider the flaring loop as a possible cause for the release of energetic electrons in a flare (see Vlahos and Papadopoulos, 1979; Emslie and Vlahos, 1980). Electrons locally accelerated inside a loop, stream towards the lower atmosphere. A portion of these electrons is reflected above the transition region and trapped inside the loop, while the rest are precipitating in the upper chromosphere losing their energy to collisions with the cool and dense plasma (see Figure 2).

We can approximate the distribution of the electrons away from the acceleration region, by a field aligned beam of the form

$$f_b(v_\perp, v_\parallel) = \left(\frac{1}{2\pi}\right)^{3/2} \frac{1}{a^3} \left(\frac{n_b}{n_o}\right) \exp\left[-\left[\frac{(v_\parallel - v_b)^2}{2a^2} + \frac{v_\perp^2}{2a^2}\right]\right] \quad (1)$$

where a is the thermal spread of the beam, v_b is the beam velocity, and $v_\parallel$ and $v_\perp$ refer to velocities along and perpendicular to the magnetic field, n_b and n_o are the densities of the beam and the background plasma. The distribution function for the reflected electrons can be approximated by

$$f_r(v_\perp, v_\parallel) = \frac{n_b}{n_o}\left(\frac{1}{2\pi}\right)^{3/2} \frac{1}{a^3} \exp-\left[\frac{(v_\parallel - v_b)^2}{2a^2} + \frac{v_\perp^2}{2a^2}\right] H[v_\perp - v_\parallel/\sigma] \quad (2)$$

where H is a step function which takes into account the loss cone anisotropy, σ is the mirror ratio defined as

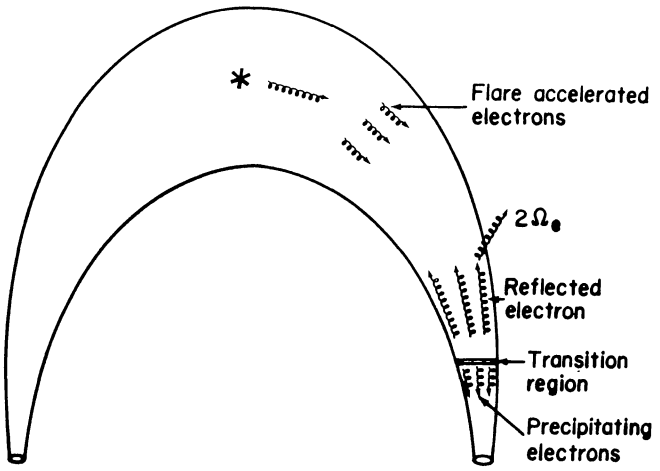

Fig. 2. A model for the magnetic field configuration of a symmetric magnetic loop. Electrons are released locally at the weak magnetic field part of the loop (e.g. at the top) and stream towards the foot where the magnetic field is strong.

$$\sigma = \left[\frac{B_{max}}{B_{min}} - 1\right]^{1/2} ,$$

and B_{max} and B_{min} are the magnetic field strength at the bottom and at the top of the loop. For numerical estimate we use the following parameters as typical of the flaring loop: $B_{max} \simeq 500G$, $B_{min} \simeq 100G$, $(v_b/c) \approx 1/3$, $(v_b/a) \approx 3.0$. Integrating equ. (2) we can find the number of reflected electrons (n_r/n_o) as a function of σ (Figure 3). We assume here that the total number of electrons in the beam is $n_b/n_o \simeq 10^{-2}$ since for $n_b/n_o \geq 10^{-2}$ (Vlahos and Papadopoulos, 1979) the beam will quasilinearly relax close to the acceleration source and never reach the foot of the loop. Note also, that $n_b/n_o \simeq 10^{-2}$ represents the total number of electron at the tail of the local Maxwellian ($v > 3\ v_e$; v_e being thermal velocity of electrons) in the acceleration source. A small electric field in the energy release region e.q. $E/E_D \lesssim 0.1$, where E_D is the local Dreicer field, can easily accelerate these electrons to 30-50 KeV. We

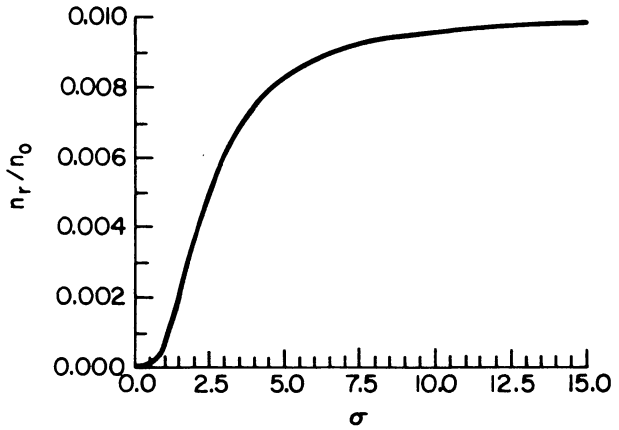

Fig. 3. The number of reflected electrons as a function of the mirror ratio σ. We asume an isotropic beam with $n_b/n_o = 10^{-2}$ and $v_{b/a} \simeq 3$.

finally assume that the length of the loop is $\simeq 10^9$ cm and its minor radius is $\simeq 10^8$ cm. The loop is assumed to be twisted inside and the magnetic field and plasma density outside are assumed smaller.

b. Plasma Effects

Before presenting detailed numerical results for the distribution function given by equ. (2) demonstrating the importance of retaining a finite (ω_e/Ω_e), we demonstrate the important physical effects by considering the maser cyclotron instability driven by a model distribution of the type $(1/2\pi v_\perp)\, n_r \delta(v_\parallel - V_\parallel)\, \delta(v_\perp - V_\perp)$. As is well known, the instability is driven by the transverse free energy $(1/2)\, n_r m V_\perp^2$ and requires the relativistic dependence of the electron mass in velocity (Chu and Hirshfield, 1978; Sprangle and Drobot, 1977; Wu and Lee, 1979). To first order in (V^2/c^2) (i.e. for mildly relativistic electrons) the resonance condition is given by

$$\omega_r - n\Omega_e\left(1 - \frac{V^2}{2c^2}\right) - k_\parallel V_\parallel = 0 \qquad (3.a)$$

ω_r is the real mode frequency, which in the weak coupling case, such as the present, should correspond to a propagating eigenmode of the ambient plasma. Therefore

$$\omega_r > \omega_x \qquad (3.b)$$

where ω_x is a cutoff frequency. From equs. (3.a) and (3.b) we find

$$k_\parallel V_\parallel + n\Omega_e\left(1 - \frac{V^2}{2c^2}\right) > \frac{1}{2}\left[\Omega_e + (\Omega_e^2 + 4\,\omega_e^2)^{1/2}\right] \qquad (4)$$

For the first harmonic and in the limit that $(\omega_e/\Omega_e) \to 0$, there is no problem satisfying this condition. However, as $(\omega_e/\Omega_e) \to 1$, this condition cannot be satisfied anymore and the instability is suppressed for n=1, since the beam can couple resonantly only to reactive (i.e. evanescent) modes. It is easy to see from equ. (4) that there is no such problem for the higher harmonics.

We estimate the relative growth of the γ_1/γ_2 as a function of ω_e/Ω_e in O- and X-mode by using the full dispersion relation given by Baldwin et al. (1969) and following the calculation of Lee and Wu (1980), for the velocity distribution given by equ. (2). The dispersion relation includes the influence of the background plasma, as well as the effect of electrostatic fields on the growth rate for both the fast extraordinary mode (X-mode) and the ordinary mode (O-mode) (see Appendix).

The results of our numerical calculations are shown in Figures 4 and 5. In Figure 4a we show the growth rate as a function of frequency near Ω_e, $2\Omega_e$, for $\omega_e/\Omega_e \simeq 0.1$ and maximized with respect to angle or equivalently $(k_\parallel/k)$. In comparing these results with respect to the limit $(\omega_e/\Omega_e) \to 0$ taken by Melrose and Dulk (1981), which gave $(\gamma_1/\gamma_2) \simeq 100$, we note that although the plasma effects are not yet very important the ratio (γ_1/γ_2) has been reduced by an order of magnitude. Figure 4b is similar to 4a but for $\omega_e/\Omega_e \simeq 0.6$. It is found that the first harmonic has

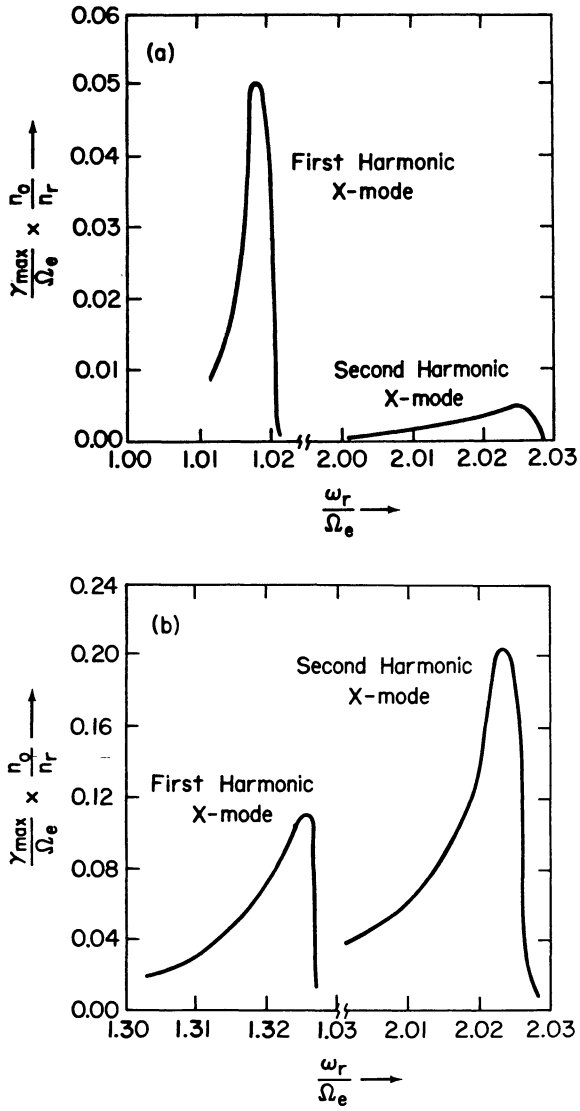

Fig. 4. (a) The variation of $(\gamma_{max}/\Omega_e) \times (n_o/n_r)$ for the first and second harmonic X-mode as a function of (ω_r/Ω_e) for (c/a) = 9, σ = 2.0 and $k_\perp a/\Omega_e \simeq 0.1$ and (b) the same for $(\omega_e/\Omega_e) \simeq 0.6$, and other parameters are the same as for figure a.

a smaller growth rate than that of the second. In Figure 5a we plot the maximum growth rate as a function of ω_e/Ω_e. We find that for $(\omega_e/\Omega_e) \gtrsim 0.4$ the second harmonic X-mode has larger growth than the first. In Figure 5b we plot the maximum growth for the first and second harmonic for the O-mode. The conclusion is that for $\omega_e/\Omega_e \gtrsim 0.4$ the fastest growing mode is the first harmonic O-mode but its growth is comparable to the growth rate of the second harmonic X-mode. The first harmonic O-mode becomes evanscent for $\omega_e/\Omega_e \gtrsim 1.025$ and growth rates vanishes. We discuss next the saturation mechanism and the implications of the relative growth between the harmonics.

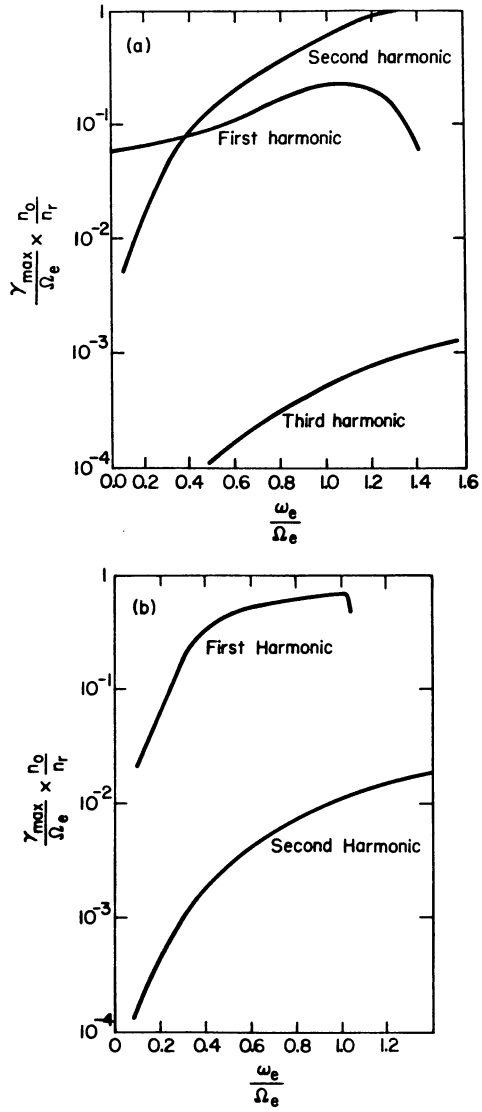

Fig. 5. (a) Shows the variation of $(\gamma_{max}/\Omega_e) \times (n_o/n_r)$ as a function of the ratio ω_e/Ω_e for the following parameters: $(v_b/a) = 3$, $(c/a) = 9$, $\sigma = 2.0$, $k_\perp a/\Omega_e \simeq 0.1$. It is found that for $\omega_e/\Omega_e \gtrsim 0.4$ the second harmonic grows faster than the first harmonic for X-mode. The third harmonic has a relatively smaller growth rate. (b) Shows the same variation for O-mode and for the same parameters. In this case 1st harmonic has larger growth rate than the 2nd harmonic for X-mode. The second harmonic for O-mode grows very slowly as compared to the first one.

c. Quasilinear Saturation of the Electron Cyclotron Maser

The amplification of the radiation is due to the presence of a positive slope in the velocity distribution function perpendicular to the magnetic field. The electromagnetic waves driven by this velocity anisotropy can pitch angle scatter the reflected electrons into the loss cone as the electrons move away from the reflection point, in the foot of the magnetic loop. We examine below the saturation of the cyclotron maser on the basis of the one-dimensional quasilinear equation (Wu et al., 1981)

$$\frac{\partial f_r}{\partial t} = \frac{1}{v_\perp} \frac{\partial}{\partial v_\perp} D_\perp \cdot [v_\perp \frac{\partial f_r}{\partial v_\perp}] \tag{5}$$

$$\frac{\partial \varepsilon_k}{\partial t} = 2\gamma \varepsilon_k \tag{6}$$

and

$$D_\perp = \frac{4\pi^2 e^2}{m^2} \int d^3k \, \varepsilon_k \, \delta[\omega_r - \Omega_e(1 - \frac{v^2}{2c^2}) - k_\parallel v_\parallel] \tag{7}$$

where $D_\perp$ is the diffusion coefficient and ε_k the wave spectral density, and γ is the growth rate of the fastest growing mode. We can solve the above equations to find the time and wave amplitude at the point where $(\partial f_r/\partial v_\perp) \simeq 0$. We can do these calculations by using the velocity distribution given by equ. (2) but the results are numerically involved and the answer not very different (a factor of 3-5) from the results obtained from Wu et al. (1981). In the later case f_r was approximated by the difference of two Maxwellians with different perpendicular energy. The saturation level is given by the equation

$$\frac{W_s}{n_o m a^2} \simeq (\frac{\Omega_e}{\omega_e})^2 (\frac{k_\parallel a}{\Omega_e}) \frac{\gamma}{\Omega_e} \tag{8}$$

For $\omega_e \simeq \Omega_e$, $(k_\parallel a/\Omega_e) \simeq 5\times10^{-2}$ we find that

$$\frac{W_s}{n_o m a^2} \simeq 5\times10^{-2} (\frac{\gamma}{\Omega_e}) \tag{9}$$

We can parenthetically remark at this point that another simple way to estimate the upper limit for the saturation level is from the total free energy (W_F) available in our "excited" distribution f_r (see Wu et al., 1981)

$$W_F = \int d^3v \, (\frac{1}{2} mv^2 - \frac{3}{2} T_o) f_r \tag{10}$$

where T_o is the effective temperature defined by

$$T_o = \frac{m}{2\pi} n_r^{2/3} \exp(-1 - \frac{2}{3n_r} \int d^3v f_r \, \ell n f_r). \tag{11}$$

We found that W_F is not very different from W_s given by equ. (8), (this was also the case in the Wu et al. (1981) calculation).

We can now use equ. (8) to estimate an approximate saturation time. The mode which saturates the instability grows as

$$I_1 = I_o \exp(\gamma_1 t_o) \tag{12}$$

where t_o is the saturation time, at saturation

$$\gamma_1 t_o \simeq |\ell n (\frac{W_s}{n_o m a^2})| \tag{13}$$

If the plasma effect are ignored and $\gamma_1/\gamma_2 \simeq 100$ the intensity in the second harmonic will be given by

$$I_2 \simeq I_0 \exp(\gamma_2 t_o) \qquad (14)$$

Using equ. (13) in equ. (14) we find

$$I_2 \simeq I_0 \exp(\beta \frac{\gamma_2}{\gamma_1}) \qquad (15)$$

where $\beta = |\ell n[W_s/n_o ma^2]|$. Thus we can easily conclude that for $\gamma_2/\gamma_1 \simeq 1/100$ and $\beta \simeq 5\text{-}8$, I_2 will barely grow above the thermal noise level.

III. THERMAL DAMPING AND GYROTHERMAL ABSORPTION FROM FLARING LOOPS

In estimating the growth rates plotted in Figures 4 and 5, we assumed that the background plasma was cold ($T_e = 0$). In this section we relax this assumption and use the full dispersion relation to estimate the damping (see Appendix). The total velocity distribution at the foot of the loop is taken as

$$f(v_\perp, v_\parallel) = f_M(v^2) + f_b(v_\perp, v_\parallel) + f_r(v_\perp, v_\parallel) \qquad (16)$$

where f_M is the local Maxwellian, f_b and f_r are given by equations (1) and (2) and represent the local population of precipitating and reflected electrons. Since f_b is isotropic in $v_\perp$ we ignore its presence in our present study. The real part of the dispersion relation is not affected by the local Maxwellian distribution but the imaginary part will be influenced by the local Maxwellian and f_r. The total growth rate is

$$\frac{\gamma_{eff}}{\Omega_e} = (\gamma_n - \gamma_{D,n})/\Omega_e \qquad (17)$$

where γ_n is the growth rate plotted in Figure 5 and $\gamma_{D,n}$ the thermal damping of the excited cyclotron mode. Equ. (17) gives a threshold condition for the excitation of the instability.

In previous studies the damping from the radiating layer was ignored (Holman et al., 1980, Melrose and Dulk, 1981). This is correct only if the frequency shift $\Delta\omega \gg k_\parallel v_e$ so that the radiation emitted at $\omega = n\Omega_e + \Delta\omega$ escapes the resonant absorption from the $n\Omega_e$ layer and the only relevant is the absorption from the $(n+1)\Omega_e$ layer. (Stepanov (1978) has also discussed the damping from the background plasma for waves with ($k_\parallel = 0$), but we found in our analysis in Section 3 that the γ_n maximizes for $k_\parallel \neq 0$., thus we repeated the calculation for $\gamma_{D,n}$ again here). In Figures 6 and 7 we demonstrate that the assumption of Holman et al. (1980) and Dulk and Melrose (1981) is incorrect since each harmonic cease to be a line around $n\Omega_e$ for $T_e \neq 0$, and in fact for temperatures $T_e \gtrsim 2.10^6$ K, the damping can easily overcome growth, stabilizing the system. We demonstrate these in Figures 6 and 7. In Figures 6a,b we plot the thermal damping for X- and O-modes at the point at which the

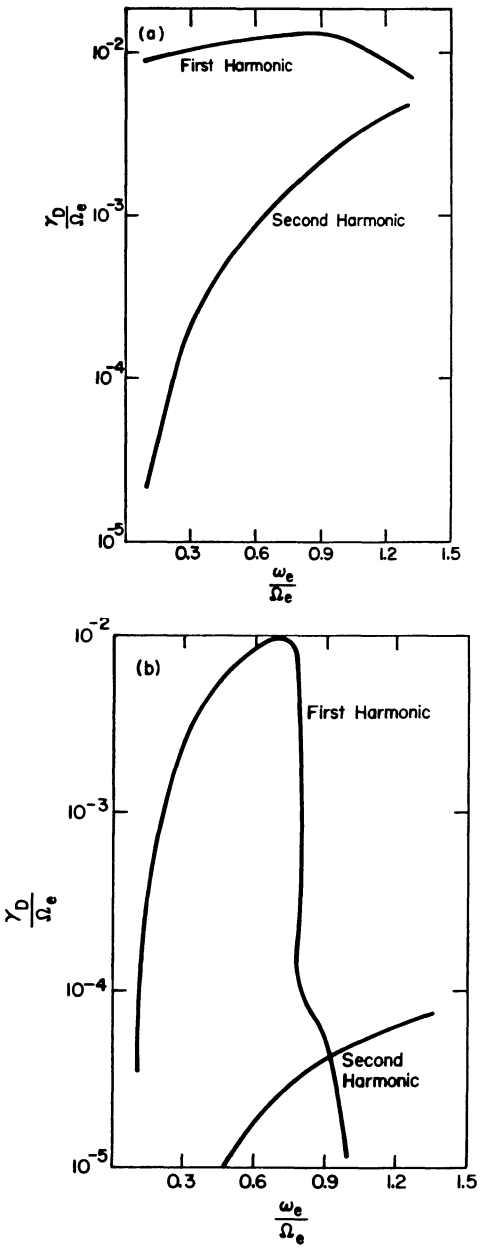

Fig. 6. The thermal damping in the first harmonics as a function of (ω_e/Ω_e). (a) for the X-mode (b) for the O-mode. $T_e = 2.0 \times 10^6$ K, while the other parameters (ω_r/Ω_e, $k_\parallel/k$ e.t.c) are the same as in Figure 5.

growth rate maximizes (e.g. we plot $\gamma_{D,n}$ for the same values of $(k_\parallel/k)$ and (ω_r/Ω_e). We assume that the initial temperature in the flaring loop is close to the coronal temperature ($\simeq 2\times10^6$ K). For first harmonic O-mode, the damping for $(\omega_e/\Omega_e) \gtrsim 0.78$ reduces significantly and therefore effective growth rate for first harmonic O-mode is about twice to that of second harmonic X-mode for $0.78 \lesssim (\omega_e/\Omega_e) \lesssim 1.02$. In Figure 7a,b we plot the γ_{eff}/Ω_e given in equation (17) as a function of ω_e/Ω_e assuming that $n_r/n_o \simeq 10^{-2}$ (e.g. total trapping of the energetic electrons in the beam). Comparing Figures (5) and (6) we can easily show that the second harmonic X-mode can have an

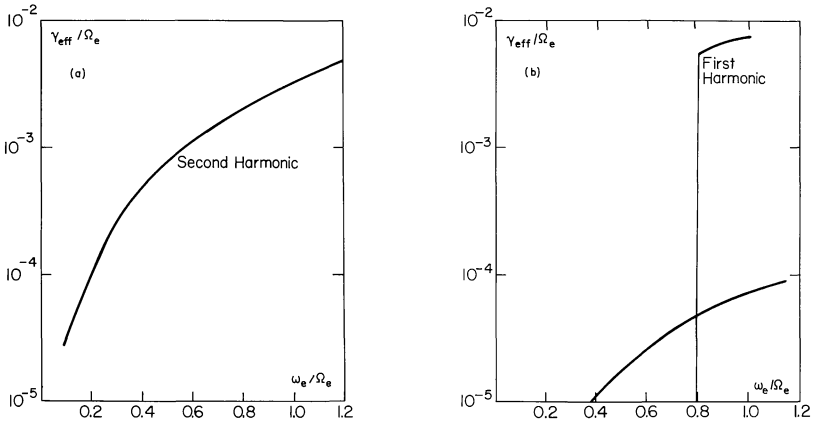

Fig. 7. The effective growth rate defined in eq. (17) as a function of (ω_r/Ω_e) for $n_r/n_o = 10^{-2}$ (total trapping). (a) for the X-mode and (b) for the O-mode.

effective growth larger than zero only if $(n_r/n_o) \geq 4\times10^{-3}$ which is close to the number of electrons we predict that will be reflected from Figures 3 if $\sigma \gtrsim 2$. From Figures (6) and (7) we can immediately see that the first harmonic in the X-mode is damped and the growth rate in the other harmonics is reduced. Before estimating the total power emitted from the cyclotron-maser in the flaring loop it is important to discuss the pecularities of the flaring loop model in relation to the thermal absorption of waves emitted at $n\Omega_e + \Delta\omega$ and absorbed from the $(n+1)\Omega_e$ level.

The thermal damping of electromagnetic waves propagating out of the corona in a magnetic field topology which decreases away from the sun's surface has been discussed extensively by Zheleznyakov (1970). His results are correct for oblique propagation in a homogeneous stratified atmosphere. Stepanov (1978), recently repeated these calculations for waves propagating perpendicular to the magnetic field ($k_\parallel = 0$) and found that the thermal absorption at $(n + 1)\Omega_e$ level is reduced by one to two orders of magnitude; that is, the angle between the electromagnetic wave and the magnetic field plays an important role in the absorption. These calculations should be further extended to include the escape of electromagnetic waves from an active region where the magnetic field is concentrated in loop-like magnetic structures and falls off quickly away from the loop. This analysis requires a simple model for the magnetic and plasma structure of the loop. We present below a qualitative picture of the gyrothermal absorption from a flaring loop for a specific model of a force free flaring loop. Sturrock and Uchida (1981) have given simple expression for the magnetic field $\vec{B}(B_r, B_\phi, B_z)$ which are solutions of the force free equations for $(r/L) \ll 1$, where r is the minor radius and L is the length of the loop, given below

$$B_z(r,z) = B_o(z) - [\tfrac{1}{4} B_o''(z) + b^2 B_o(z)]\, r^2$$
$$B_r(r,z) = -\tfrac{1}{2} B_o'(z)\, r \qquad (18)$$
$$B_\phi(r,z) = b\, B_o(z) r$$

and b is constant. The magnetic structure given in eq. (18) serves only to illustrate our qualitative arguments below. In a flaring loop, by definition, B_z, B_r, and B_ϕ are very different from the ones given in eq. (18), e.g. the twist of the magnetic lines is larger. In Section 2 we adopted a scale length of a compact flaring loop as $\simeq 10^9$ cm along z and 10^8 cm along r. Using this geometry we can draw the resonance layers for any single frequency observation (e.g. for f = 3GHz the resonant layers for the first three harmonics are drawn in Figure 8). The width in these lines represents the bandwidth in the emission or the bandwidth in the receiver, whatever is larger. We may now make several comments related to the absorption of the electromagnetic waves emitted close to $n\Omega_e$ in a flaring loop:

a. For frequencies $f \gtrsim 3$GHz the first harmonic layer corresponds to a magnetic field $B \geq 1000$ Gauss, which is (according to our initial model) below or very close to transition region where of course T_e decreases but the collisional damping (not included in our calculation) increases dramatically.

b. An electromagnetic wave emitted from the layer $n\Omega_e$ with an initial angle ϕ_1 will approach the $(n+1)\Omega_e$ layer at a different angle ϕ_2 since the magnetic field is changing as a function of (z,r). At the level $(n + 1)\Omega_e$ the energy carried by the wave will be damped or amplified depending on the value of γ_{eff} at the specific point (e.g. see Figure 8). We believe that in a flaring loop the structure of the $n\Omega_e$ layers changes dynamically and in so doing ϕ_1, ϕ_2 and γ_{eff} which determine the total power escaping from the loop (for the cyclotron maser as well as for the gyrosynchrotron radiation) also changes. The analysis of the role of the magnetic field geometry in the microwave radiation escaping from the loop is currently in preparation.

c. Waves around $n\Omega_e$ emitted with large ϕ_2 will cross the layer $(n + 1)\Omega_e$ at the edge of the loop where $L_B \simeq B(r)(dr/dB)$ is small ($\lesssim 10^8$ cm) and the attenuation is much smaller than the values quoted by Zheleznyakov (1970). Outside the loop the electromagnetic wave propagates with very little loss of energy, unless it crosses another loop with strong magnetic field before reaching the observer.

Before closing this section it is worth commenting

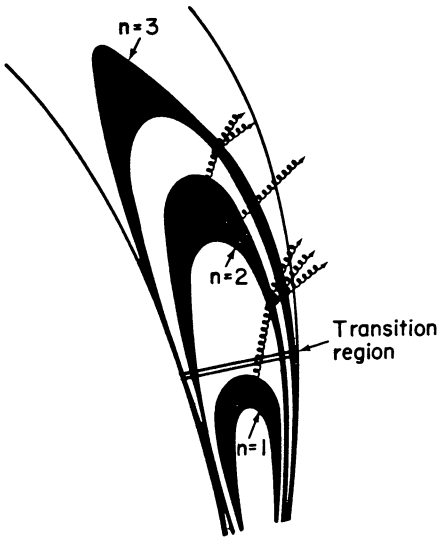

Fig. 8. A schematic representation of the cyclotron harmonic resonance layer for f > 3GHz. The width of the resonance layer depends on the magnetic scale gradient, and since L_R = B(dz/dB) >> L_r = B(dr/dB) the resonance layer is broaden along the z direction.

that for $T_e \simeq 10^7$ K most of the emission in the first and second harmonic is damped and the cyclotron maser is, unable to explain the high brightness sources discussed here.

IV. ESTIMATED POWER RECEIVED AT THE EARTH FROM A FLARING LOOP MASERING IN LOWEST HARMONICS

The observations with high time resolution instruments are not complete yet. They are currently available only for a few isolated frequencies. Slottje (1978) summarizes their basic characteristics at 2.65 GHz and his analysis is used here to estimate the power expected from the above model. The power received at the earth from a masering flaring loop is given by the formula

$$P = (W_s V_{gr}) \frac{A}{4\pi R_o^2 \Delta f} \qquad (19)$$

where A is the surface area of the source, R_o is the distance of the source from the earth $\simeq 1.5 \times 10^{13}$ cm, W_s is given from eq. (9) by using the (γ_{eff}/Ω_e), Δf is the bandwidth reported from Slottje's observations, and V_{gr} is the group velocity of the electromagnetic wave. An estimate of the source area A is found by assuming that the energetic electrons moves a distance $D = V_{ex} \cdot t_o$, along the field lines where t_o is the saturation time for the maser. For $V_{ex} \lesssim v_b = 10^{10}$ cm/sec and $t_o \simeq 100$ μsec, D will be of the order of 10-100 km. From eq. (15) we find that

$$P \lesssim 10^{-17} \text{ Watts m}^{-2} \text{ Hz}^{-1} \qquad (20)$$

for $A = D \cdot r$, where r is the radius of the loop, $(n_r/n_o) = 4 \times 10^{-3}$ given in Figure 3 for σ=2, $\Delta f \simeq 100$ MHz, and $\omega_e \simeq \Omega_e$. This power is comparable to the value quoted from Figure 1 at the peak of the spiky component.

In answering the question as to whether the radiation is polarised and whether it is O-mode or X-mode one must go back to the analysis made in Section 3 regarding the absorption or amplification of the radiation as it crosses the $(n+1)\Omega_e$ layer. We can outline two different scenarios for the emission which will give different polarizations but comparable power to the one estimated by equ. (20).

a. The first harmonic layer for $f = f_{obs} = 2.65$ GHz is at the transition region and the emission at $\omega = \Omega_e + \Delta\omega$ is damped. Then, the second harmonic layer radiates at $\omega = 2\Omega_e + \Delta\omega$ which suffers little if any absorption of $3\Omega_e$, and escapes from the loop. In this case the received radiation is nearly 100% polarized in the X-mode.

b. The first harmonic layer is above the transition region and the ray emitted at $\omega = \Omega_e + \Delta\omega$ from the O-mode approaches the $2\Omega_e$ layer at a point where $\gamma_{eff}(2\Omega_e) > 0$ thus the wave is amplified before it escapes from the loop. But at the same time nothing can prevent the $\omega = 2\Omega_e + \Delta\omega$ radiation from the X-mode to escape too. In this case the radiation is partially polarized, since $W_s/n_o m a^2$ for the first harmonic O-mode and second harmonic X-mode are not very different (See Figure 7). This is in good agreement with the observations since Slottje (1980) reported highly polarized as well as unpolarized spikes.

In estimating the efficiency of the emitted power we use eq. (9) to estimate the ratio, $(W_s/n_b \varepsilon_b) \simeq 0.1\%$; thus by radiating only 0.1% of the beam energy we can explain the observed high brightness sources in the sun (brightness temperature $\simeq 10^{15}$ K), and their polarization.

V. DISCUSSION

We examined the cyclotron maser instability in a flaring loop. According to the flare model proposed in Section II, mildly relativistic electrons released at the top of the magnetic loop (where the magnetic field is weak) stream toward the chromosphere where they are reflected by the strong magnetic field at the foot of loop back into the corona. Electrons with $v_\parallel$ large on the other hand have reflection points inside the chromosphere and loose their energy collisionally before returning back into the corona. Thus the velocity distribution for the reflected electrons has an anisotropy in $v_\perp$ which can drive the cyclotron maser. In this analysis we included (a) the role of the background plasma (b) the role of the thermal damping and (c) the importance of the magnetic field structure of the loop. Holman et al. (1980) and Melrose and Dulk (1981) have ignored the above effects and arrived at different results. We summarize our conclusions below.

1. Our analysis demonstrated that if the first harmonic in a particular point of the loop grows faster than the second harmonic the maser will saturate before the second harmonic grows above the thermal noise level. However, including finite (ω_e/Ω_e) ratios, the ratio γ_1/γ_2 is reduced and in fact becomes less than one at $\omega_e/\Omega_e \simeq 0.4$ for the X-mode. For the O-mode $\gamma_1/\gamma_2 >> 1$ but γ_1(O-mode) $\geq \gamma_2$(X-mode) so the first harmonic O-mode may still saturate the maser while I_2

grows at a comparable rate with the first harmonic and can easily reach high values.

2. Our study included the thermal damping in each harmonic and estimated the γ_{eff} as a function of ω_e/Ω_e. We found that for 2×10^6 K the first harmonic in the X-mode is damped and the growth rates of the $2\Omega_e$ in the X-mode as well as the Ω_e and $2\Omega_e$ in the O-mode are reduced. We notice that a relatively large number of electrons need to be reflected for the $\gamma_{eff} > 0$. For temperatures larger than $T_e \gtrsim 5\times10^6$ K the damping is so severe that cyclotron masering ceases to be an attractive radiation process for high brightness temperature sources in the sun.

3. We discussed qualitativily the role of the magnetic field topology on the structure of the resonance layer at Ω_e, $2\Omega_e$ and $3\Omega_e$. We also stressed the fact that in flaring loops $L_B(r) = B(dr/dB)$ is small and that if $\gamma_{eff} > 0$ at the $(n+1)\Omega_e$ layer the radiation emitted at $n\Omega_e + \Delta\omega$ will be amplified instead of absorbed.

4. The estimated power from the second harmonic X-mode and the first harmonic O-mode can easily account for the observed radiation. We suggested that if O-mode does not escape, the radiation will be highly polarized in the extraordinary mode, but in the case that O-mode escapes as well the radiation will be partially polarized.

5. We also found that our conclusions are not sensitive to the form of f_r as long as $\partial f_r/\partial v_\perp$ is positive.

In our analysis above we did not discuss the mechanism which causes the spiky structure of the burst. We found that saturation time is much faster than the observed duration of the spike. The cause of the spiky behavior is still an open question which must be addressed independently. This work is currently in preparation.

We may then conclude that the two components in Figure 1 e.g. the "smooth" and the "spiky" could be caused by two different emission mechanisms operating simulataneously (a) gyrosynchrotron emission from the trapped electrons (see Ramaty, 1969; Takakura, 1972) and (b) the cyclotron-maser from the reflected electrons. Although we offer no explanation for the mechanism which causes the spikes we suggest that the abrupt reduction of the spiky component at the maximum of the smooth pulse (see Figure 1a) is caused by the gradual increase of the temperature of the ambient plasma above 2×10^6 K which causes a large reduction in γ_{eff}. Finally we like to stress that only flaring loops with plasma parameters $\omega_e/\Omega_e > 0.4$, in the rising part of the impulsive phase, where $T_e \lesssim 2\times10^6$ K can be candidates for cyclotron maser emission.

ACKNOWLEDGEMENTS

The authors want to thank Prof. C. S. Wu and Dr. M. L. Goldstein for fruitful and stimulating discussions. The present research was supported by NASA grant NAG W-81. Our numerical computations were partially supported by the Computer Science Center of the University of Maryland.

Appendix

The basic equation which we solved to obtain the growth rate is

$$\gamma_{\pm} = -\left.\frac{I_m D(\omega_r,\underline{k})}{\frac{\partial}{\partial\omega_r}\,\mathrm{Real}\,D(\omega_r,\underline{k})}\right|_{N^2 = N_{\pm}^2} \qquad (A.1)$$

where + and − signs corresponds to the ordinary and the extraordinary mode, N is the refractive index and $\mathrm{Im}D(\omega_r,\underline{k})$ is given by

$$I_m D(\omega_r,\underline{k}) = S_{xx} I_m \varepsilon^r_{xx} + S_{yy} I_m \varepsilon^r_{yy} + S_{zz} I_m \varepsilon^r_{zz} + S_{xy} R_e \varepsilon^r_{xy} + S_{xz} I_m \varepsilon^r_{xz} + S_{yz} R_e \varepsilon^r_{yz} + S_{zx} I_m \varepsilon^r_{zx} + S_{zy} R_e \varepsilon^r_{zy},$$

$$S_{xx} = N^4 \sin^2\theta - N^2(a_1 \sin^2\theta + a_2) + a_1 a_2$$

$$S_{yy} = -N^2(a_1 \sin^2\theta + a_2 \cos^2\theta) + a_1 a_2$$

$$S_{zz} = N^4 \cos^2\theta - N^2 a_1 (1 + \cos^2\theta) + a_1^2 - a_3^2$$

$$S_{xy} = 2a_3(a_2 - N^2 \sin^2\theta)$$

$$S_{xz} = S_{zx} = N^2(N^2 - a_1) \sin\theta \cos\theta$$

$$S_{yz} = S_{zy} = N^2 a_3 \sin\theta \cos\theta$$

$$a_1 = 1 - \frac{\omega_e^2}{\omega_r^2 - \Omega_e^2}$$

$$a_2 = 1 - \frac{\omega_e^2}{\omega_r^2}$$

$$a_3 = \frac{\omega_e^2 \Omega_e}{\omega_r(\omega_r^2 - \Omega_e^2)}$$

θ denotes angle between $\underline{k}$ and $\underline{B}_s$. In Real $D(\omega_r,\underline{k})$ we may ignore the contribution from the reflected electrons (see Lee and Wu, 1980). $\mathrm{Im}\varepsilon^r_{ij}$ and $\mathrm{Re}\varepsilon^r_{ij}$ are the imaginary and real part of the dielectric tensor obtained from Harris (1968) by using equ. (2) for the unstable velocity distribution.

In estimating the damping from a Maxwellian background plasma we can show that

$$\frac{\gamma_{D,n}}{\Omega_e} = (\pi/2)^{1/2} \left(\frac{\omega_e}{\omega_r}\right)^2 \left(\frac{\omega_r}{\Omega_e}\right) \left[\sum_n \left(\frac{\omega_r}{k_\parallel v_e}\right) \exp - \frac{(\omega_r - n\Omega_e)^2}{2k_\parallel^2 v_e^2}\right.$$

$$\{S_{xx} A_{xx} + S_{yy} A_{yy} + S_{zz} A_{zz} + S_{xy} A_{xy} + 2S_{xz} A_{xz}\}/(\omega_r \frac{\partial D_r}{\partial \omega} (\omega_r, \underline{k}))] \Big|_{N^2 = N_{\pm}^2}$$

where

$$A_{xx} \simeq A_{yy} \simeq A_{xy} = (\frac{1}{2})^n (\frac{k_\perp v_e}{\Omega_e})^{2n-2} \frac{n}{(n-1)!}$$

$$A_{zz} = (\frac{1}{2})^n (\frac{k_\perp v_e}{\Omega_e})^{2n} \frac{(\omega_r - n\Omega_e)^2}{k_\parallel^2 v_e^2} \frac{1}{n!}$$

$$A_{xz} = (\frac{1}{2})^n (\frac{k_\perp v_e}{\Omega_e})^{2n-1} \frac{(\omega_r - n\Omega_e)}{k_\parallel v_e} \frac{n}{n!} .$$

REFERENCES

Baldwin, D.E., Bernstein, I.B., and Weenink, M.P.H., 1969, Advances in Plasma Physics, edit. by W. B. Thompson and A. Simon, 3, p. 32, Wiley, New York.

Chu, K.R., and Hirshfield, J.L., 1978, Phys. of Fluids, 21, 461.

Emslie, A.G., and Vlahos, L., 1980, Ap.J., 242, 359.

Fung, P.C.W., and Yip, W.K., 1966, Australian J. Physics, 19, 759.

Harris, E.G., 1968, Physics of Hot Plasma, edited by B. J. Rye and J. C. Taylor, Plenum Press, New York.

Holman, G.D., Eichler, D. and Kundu, M.R., 1980, in IAU Symp. 86, Radio Physics of the Sun, edit. by M. Kundu and T. Gergely (Dordrecht: Reidel) p. 195.

Kaufman, P., Strauss, F.M., and Opher, R., 1980, IAU Symp 86, Radio Physics of the Sun, ed. by M.R. Kundu and T. Gergely (Dordrecht: Reidel), p. 205.

Kundu, M.R., and Vlahos, L., 1982, Space Science Reviews, (in press).

Lee. L.C., and Wu, C.S., 1980, Physics of Fluid, 23, 1348.

Mangeney, A., and Veltri, P. 1976, Astron. Astrophys., 47, 165.

Melrose, D.B., and Dulk, G.A., 1981, Electron Cyclotron Maser as the Source of Certain Solar and Stellar Radio Bursts, Univ. of Colorado, Boulder, preprint.

Ramaty, R., 1969, Ap.J., 178, 241.

Slottje, C., 1978, Nature, 275, 520.

Slottje, C. 1980, in IAU Symposium 86, Radio Physics of the Sun, edt. by M. Kundu and T. Gergely (Dordrecht: Reidal), p. 195.

Sprangle, P., and Drobot, A.T., 1977, IEEE Trans. Microwave Theory Tech., 25, 528.

Stepanov, A.V., 1978, Sov. Astron. Lett., 4, 103.

Sturrock, P. and Uchida, Y., 1981, Ap. J., 233, 717.

Takakura, T., 1972, Solar Physics, 26, 151.

Twiss, R.Q., and Roberts, J.A., 1958, Australian J. Phys., 11, 424.

Vlahos, L. and Papadopoulos, K., 1979, Ap. J., 246, 331.

Wu, C.S., and Lee, L.C. 1979, Astrophys. J., 230, 621.

Wu, C.S., Tsai, S.T., Xu, M.J., and Shen, J.W., 1981, Ap. J., 248, 384.

Zheleznyakov, V.V., 1970, Radio Emission of the Sun and Planets (Oxford: Pergamon Press).